

**Elastic anomalies in Ag-Zn alloys**

B. Magyari-Köpe and G. Grimvall

*Theory of Materials, Physics Department, Royal Institute of Technology, Stockholm Center for Physics, Astronomy and Biotechnology, SE-106 91, Stockholm, Sweden*

L. Vitos

*Applied Materials Physics, Department of Materials Science and Engineering, Royal Institute of Technology, SE-100 44 Stockholm, Sweden**and Research Institute for Solid State Physics and Optics, P.O. Box 49, H-1525 Budapest, Hungary*

(Received 1 March 2002; revised manuscript received 29 April 2002; published 23 August 2002)

*Ab initio* total energy calculations, based on the *exact muffin-tin orbitals theory*, are used to determine elastic properties of  $\text{Ag}_{1-c}\text{Zn}_c$  random alloys in the face-centered and body-centered cubic crystallographic phases. The compositional disorder is treated within the framework of the *coherent potential approximation*. The cubic elastic constants  $B$ ,  $C'$ , and  $C_{44}$  and the Debye temperatures are calculated for the whole range of concentrations,  $0 \leq c \leq 1$ . Experimental data are in very good agreement with the present results. Rapid variations of  $C'$  and  $C_{44}$  are observed at high Zn concentrations, which contradicts the common empirical observation that alloying has only minor effects on elastic properties.

DOI: 10.1103/PhysRevB.66.064210

PACS number(s): 62.20.Dc, 71.15.Nc, 71.20.Be, 61.66.Dk

**I. INTRODUCTION**

An important aspect of *ab initio* electron structure calculations in solids is that they can be applied to conditions which are inaccessible to experiments. In many cases they have reached an accuracy comparable to that of experiments, and thus can give new insight into the physics of solids. One early such example is the systematic calculation of the elastic constants of metallic elements<sup>1,2</sup> in face-centered-cubic (fcc) and body-centered-cubic (bcc) lattices. In contrast, very little is known about the elastic properties of *A-B* binary metallic alloys for the entire range of concentrations of the elements *A* and *B* in a given lattice structure. The solubility of *A* in *B*, and vice versa, is usually limited (cf. Fig. 1), and even in the thermodynamically stable range of concentrations the experimental information is meagre.<sup>3</sup> At the theoretical level, most investigations of random alloys have been limited to the study of the energy differences of competing crystallographic phases and the bulk modulus. Recent progress<sup>4</sup> in the *ab initio* description of metallic alloys has made it possible to extend the calculations of elastic constants from ordered structures to the case of random substitutional alloys of any concentration. These theoretical developments allow one to study the thermodynamically stable and metastable phases of random alloys and facilitate to achieve a deep understanding of the dynamical stability and instability at different concentrations of alloying elements.

It is the purpose of this paper to give a detailed account of the elastic properties of Ag-Zn binary alloys. The Ag-Zn alloy is a prototype of the noble-metal-divalent-metal (Zn, Cd) Hume-Rothery systems. The crystal structures and the solubility limits of Hume-Rothery intermediate phases were proposed<sup>5</sup> to correlate with the number of the valence electrons per atom (1 for the noble metal and 2 for Zn, Cd). Thus, an extensive study of the Ag-Zn binary alloy can promote a general description and comprehension of the properties of this important class of material. Here we present the

elastic constants of  $\text{Ag}_{1-c}\text{Zn}_c$  for  $0 \leq c \leq 1$  in the fcc and bcc lattice structures. A very good agreement with experiments is obtained for the thermodynamically stable phases—i.e., the fcc phase for  $c \leq 0.4$  and bcc phase for  $c \approx 0.5$ ; cf. Fig. 1. In ranges of concentrations that cannot be reached experimentally we find large and rapid variations in elastic shear moduli. This result contradicts the empirical observation that alloying has only a small effect on elastic properties, except for some magnetic systems.<sup>3</sup> Another important aspect is that of dynamical (mechanical) stability. For instance, pure Ag crystallizes in the fcc structure. Many models in materials science assume that other structures, e.g., the bcc or hexagonal-close-packed (hcp) lattices, would represent possible thermodynamically metastable phases of Ag. We find that bcc  $\text{Ag}_{1-c}\text{Zn}_c$  is dynamically unstable under shear for  $c \geq 0.76$  and is almost unstable for small  $c$ . Similarly, the fcc

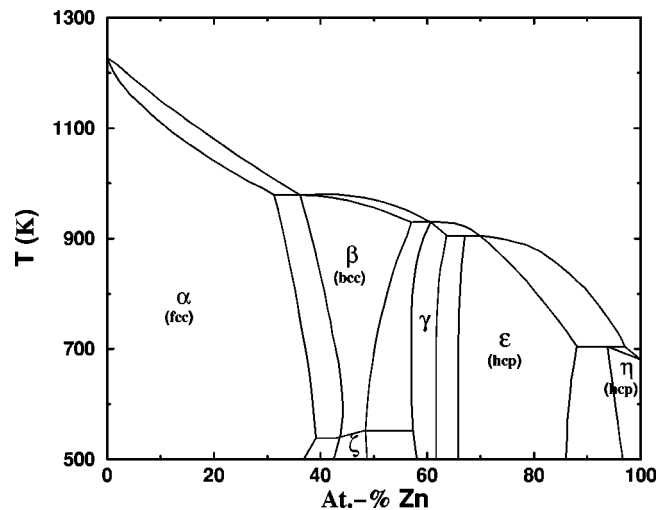


FIG. 1. The essential parts of the Ag-Zn phase diagram (Ref. 39).

phase is at the verge of being dynamically unstable at the Zn-rich end.

The present *ab initio* total energy study is based on the *density functional theory*.<sup>6</sup> The Kohn-Sham equations<sup>7</sup> are solved using the recently developed *exact muffin-tin orbitals* theory,<sup>8–13</sup> and the problem of substitutional disorder is treated within the *coherent potential approximation*.<sup>4,14–16</sup> For the total energy calculation we employ the *full charge density* technique.<sup>13,17</sup>

The rest of the paper is divided into two main sections and a conclusion. Section II presents the theoretical tools. This includes a brief description of the elastic properties and lattice stability, an overview of the *ab initio* electronic structure calculation method, and the most important details of the numerical simulations. The results are presented and discussed in Sec. III.

## II. THEORY

### A. Elastic properties

The elastic properties of crystals are described by the elements  $C_{ij}$  of the elasticity tensor. In the case of cubic lattice symmetry, there are three independent elastic constants  $C_{11}$ ,  $C_{12}$ , and  $C_{44}$ . Often elastic data are presented as the bulk modulus  $B=(C_{11}+2C_{12})/3$  and the two shear moduli  $C_{44}$  and  $C'=(C_{11}-C_{12})/2$ . Dynamical (mechanical) stability requires<sup>18</sup> that

$$C_{44}>0, \quad C'>0, \quad B>0. \quad (1)$$

The elastic anisotropy can be described by the anisotropy parameter

$$A_E = \frac{C_{11} - C_{12} - 2C_{44}}{C_{11} - C_{44}}, \quad (2)$$

introduced by Every.<sup>19</sup> For an isotropic crystal  $A_E=0$ . From the three elastic constants one obtains the sound velocity  $v_s(\theta, \phi)$  for the longitudinal ( $s=L$ ) and the two transverse ( $s=T_1, T_2$ ) branches. The average of  $v_s^{-3}(\theta, \phi)$  over all directions  $(\theta, \phi)$  gives the sound velocity  $v_D$ , viz.,

$$v_D^{-3} = \frac{1}{12\pi} \sum_s \int v_s^{-3}(\theta, \phi) \sin \theta d\theta d\phi,$$

which is used in the conventional Debye model with the Debye temperature defined as

$$\theta_D = (6\pi^2/\Omega_a)^{1/3} (\hbar/k_B) v_D. \quad (3)$$

Here  $\Omega_a$  is the atomic volume, and  $\hbar$  and  $k_B$  are the Planck and Boltzmann constants, respectively. This Debye temperature determines, e.g., the low-temperature limit of the heat capacity per atom,  $C_D(T) = (12\pi^4/5)k_B(T/\theta_D)^3$ . However, in thermodynamic applications one is usually interested in high-temperature properties. Then the entropy  $S$ —and hence also the Helmholtz energy  $F$ —depends on the logarithmic average of all the phonon frequencies. In a Debye-model description of  $S$  one should use the logarithmic average  $v_{\log}$  of the sound velocities  $v_s(\theta, \phi)$  and an entropy-related Debye temperature<sup>20</sup>

$$\theta_{D,\log} = (6\pi^2/\Omega_a)^{1/3} (\hbar/k_B) v_{\log}. \quad (4)$$

Only in the simplest textbook version of a Debye model is  $\theta_D = \theta_{D,\log}$ .

At concentrations where the stability requirements (1) are violated,  $\theta_D$  and  $\theta_{D,\log}$  cannot be defined. Let  $c_{\text{crit}}$  be the concentration where the lattice becomes unstable. If one approaches  $c_{\text{crit}}$  from the stable region, the divergence of the average  $v_s^{-3}(\theta, \phi)$  makes  $\theta_D \rightarrow 0$ . However, a logarithmic singularity is so weak that  $\theta_{D,\log}$  has a finite limit as  $c \rightarrow c_{\text{crit}}$ .

### B. *Ab initio* calculation

The *exact muffin-tin orbitals* (EMTO) theory and the self-consistent implementation of this theory, within the spherical cell approximation, may be found in Refs. 8–11 and 12,13, respectively. A comprehensive description of the total energy calculation method, based on the *full charge density* technique<sup>17</sup> and the EMTO theory, is presented in Ref. 13. The application of the *coherent potential approximation* (CPA)<sup>14,15</sup> to the compositional and/or magnetic disorder, formulated in the framework of the EMTO theory, is demonstrated in Refs. 4 and 16. Here we overview the most relevant features of the EMTO-CPA method and outline some important numerical details.

The EMTO theory is an improved *screened Korringa-Kohn-Rostoker* (KKR) method, where the exact one-electron potential is represented by large overlapping potential spheres. Inside the potential spheres the potential is spherically symmetric, and it is constant between the spheres. By using overlapping spheres one describes more accurately the exact crystal potential, when compared with the conventional muffin-tin or nonoverlapping approach. The radii of the potential spheres, the spherical potentials inside the spheres, and the constant value from the interstitial are determined by minimizing (a) the deviation between the exact and overlapping potentials and (b) the errors coming from the overlap between spheres.

The EMTO's are defined for each lattice site and for each angular momentum quantum number  $L \equiv (l, m)$  with  $l \leq l_{\text{max}}$  (usually  $l_{\text{max}}=3$ ). They are constructed from the *screened spherical waves*, which are solutions of the wave equation with boundary conditions given in conjunction with nonoverlapping hard spheres.<sup>8</sup> Inside the potential spheres the low- $l$  ( $l \leq l_{\text{max}}$ ) projections of the orbitals onto the spherical harmonics  $Y_L(\hat{r})$  are the partial waves.<sup>8</sup> The matching between the screened spherical waves and the partial waves is realized by additional free-electron solutions.<sup>8</sup>

The Kohn-Sham equations are solved for the optimized overlapping potential using the Green function formalism. In the case of substitutionally disordered alloys the average alloy density of states for the energy  $z$  is determined from the average Green function<sup>4</sup>

$$\langle G(z) \rangle = \tilde{g}(z) \dot{S}(z) - \sum_i c^i [g^i(z) \dot{D}^i(z) + G_0^i(z)], \quad (5)$$

where  $c^i$  is the concentration of the alloy component  $i$ . For the sake of simplicity the site and angular momentum indices

in Eq. (5) have been omitted.  $\dot{S}(z)$  and  $\dot{D}^i(z)$  denote the energy derivative of the slope matrix and the logarithmic derivative function of the alloy component  $i$ , respectively.  $G_0^i(z)$  is the on-site component of the EMTO Green function. For definitions see Refs. 8, 13, and 16. The coherent Green function  $\tilde{g}(z)$  and the Green functions for alloy components,  $g^i(z)$ , are determined from the self-consistent solution of the CPA equations.<sup>4</sup> In Eq. (5) the first term corresponds approximately to the average density of states from the interstitial, while the second term gives the contribution from the spheres centered on each alloy component. Note that the first term has a multicenter form<sup>16</sup> and is not projected onto the alloy components. Within the single-site approximation to the impurity problem, the EMTO-CPA Green function (5) leads to an exact density of states for the optimized overlapping potential.

The complete nonspherically symmetric charge density of each alloy component is represented in one-center form around the lattice sites, i.e.,

$$n^i(\mathbf{r}) = \sum_L n_L^i(r) Y_L(\hat{r}). \quad (6)$$

The above one-center expansion can formally be obtained from the real-space expression of the average Green function,  $\langle G(z, \mathbf{r}, \mathbf{r}) \rangle = \sum_i c^i G^i(z, \mathbf{r}, \mathbf{r})$ . To this end one needs to transform the interstitial term from Eq. (5) to one-center form. However, due to this transformation, the angular momentum expansion of  $G^i(z, \mathbf{r}, \mathbf{r})$ , and thus of  $n^i(\mathbf{r})$ , will include the high- $l$  terms as well. In practice these terms are truncated at  $l_{\max}^h = 8-12$ .

Finally, the total energy of the random alloy is calculated as<sup>4</sup>

$$\begin{aligned} E_{tot} = & \frac{1}{2\pi i} \oint z \langle G(z) \rangle dz - \sum_i c^i \int v_o^i(\mathbf{r}) n^i(\mathbf{r}) d\mathbf{r} \\ & + F_{inter}[n^i] + \sum_i c^i (F_{intra}^i[n^i] + E_{xc}^i[n^i]) \\ & - \sum_i c^i \frac{\alpha_c}{w} \left( Q^i - \sum_i c^i Q^i \right)^2, \end{aligned} \quad (7)$$

where  $v_o^i(\mathbf{r})$  is the overlapping potential for the alloy component  $i$ , and  $F_{inter}$  is the average Madelung energy.  $F_{intra}^i$  and  $E_{xc}^i$  are the electrostatic and exchange-correlation energies of the alloy component  $i$  due to the charges from the Wigner-Seitz cell. The last term in Eq. (7) is the correction to the electrostatic energy calculated within the *screened impurity model*,<sup>22</sup>  $\alpha_c \approx 0.6$ ,  $w$  is the average atomic radius, and  $Q^i$  denotes the total number of electrons inside the cell for the alloy component  $i$ . The individual energy functionals are evaluated using the full charge density technique.<sup>17</sup>

The accuracy of the EMTO-CPA method has been demonstrated for the ground state properties of metals, semiconductors and oxides,<sup>23-26</sup> and binary-ordered<sup>12</sup> and random alloys.<sup>4</sup>

### C. Details of the numerical calculations

In the present application of the EMTO-CPA method to the Ag-Zn binary system the one-electron equations were solved within the scalar-relativistic and frozen-core approximations. We note that the semicore states of Ag ( $4p^6$ ) and Zn ( $3p^6$ ) are far below the valence states (Ag  $4d, 5s$  and Zn  $3d, 4s$ ). Therefore, we expect that the errors due to the unrelaxed core states are negligible in the equilibrium properties of Ag-Zn alloys. The Green function was calculated for 16 complex energy points distributed exponentially on a semi-circular contour.

In the EMTO basis set we included  $s$ ,  $p$ ,  $d$ , and  $f$  orbitals and in the one-center expansion of the full charge density (6), we used  $l_{\max}^h = 10$ . The total energy functional was evaluated by the shape function technique.<sup>17</sup> The conventional Madelung energy was calculated for  $l_{\max}^m = 8$ . The exchange-correlation term was treated within the local density approximation (LDA).<sup>27</sup> Finally, to obtain the accuracy needed for the calculation of elastic constants in the irreducible wedge of the Brillouin zones we used 30 000–50 000  $k$  points, depending on the particular crystal symmetry.

At each concentration the theoretical equilibrium volume and the bulk modulus were determined from an exponential Morse-type function<sup>28</sup> fitted to the *ab initio* total energies of fcc and bcc structures for five different atomic volumes. In order to obtain  $C'$  and  $C_{44}$  we used volume conserving tetragonal and orthorhombic deformations, i.e.,

$$\begin{aligned} D_t = & \begin{pmatrix} 1 + \varepsilon_t & 0 & 0 \\ 0 & 1 + \varepsilon_t & 0 \\ 0 & 0 & \frac{1}{(1 + \varepsilon_t)^2} \end{pmatrix}, \\ D_o = & \begin{pmatrix} 1 + \varepsilon_o & 0 & 0 \\ 0 & 1 - \varepsilon_o & 0 \\ 0 & 0 & \frac{1}{1 - \varepsilon_o^2} \end{pmatrix}, \end{aligned} \quad (8)$$

respectively. We calculated the total energies  $E(\varepsilon_t)$  and  $E(\varepsilon_o)$  for five tetragonal,  $\varepsilon_t = -0.02, -0.01, \dots, 0.02$ , and six orthorhombic,  $\varepsilon_o = 0.00, 0.01, \dots, 0.05$ , distortions. In Fig. 2 we show  $\Delta E(\varepsilon_o^2) \equiv E(\varepsilon_o) - E(0)$  in the case of pure Ag, Zn and  $\text{Ag}_{0.1}\text{Zn}_{0.9}$ ,  $\text{Ag}_{0.9}\text{Zn}_{0.1}$  alloys in the bcc crystal phase, respectively. While for Ag-rich alloys the  $\varepsilon_o^2$  dependence is nearly linear, the curvature of the total energy indicates a trend towards negative values of  $C_{44}$  for Zn-rich alloys. Therefore, the  $C_{44}$  elastic constants were determined from a second-order polynomial in  $\varepsilon_o^2$  fitted to the total energy differences  $\Delta E(\varepsilon_o^2)$ . In the case of  $D_t$ , which is an asymmetric deformation, we used a third-order polynomial fit to  $\Delta E(\varepsilon_t) \equiv E(\varepsilon_t) - E(0)$ .

### III. RESULTS AND DISCUSSION

In this section we demonstrate the application of the EMTO-CPA method to the  $\text{Ag}_{1-c}\text{Zn}_c$  random alloys. We

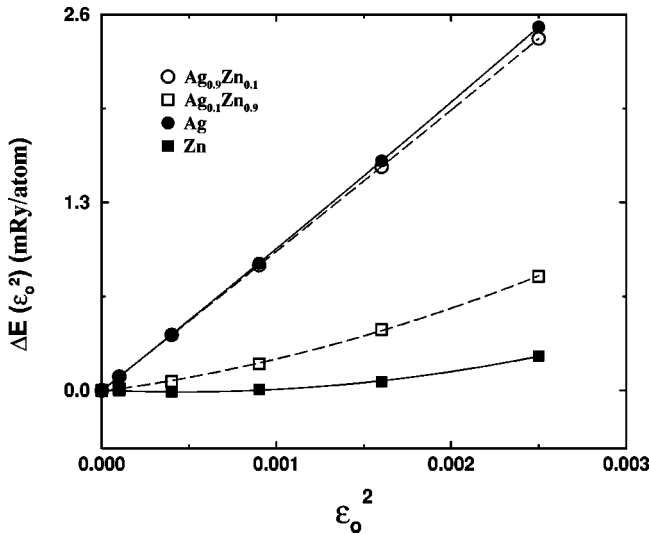


FIG. 2. The effect of orthorhombic distortion ( $\varepsilon_o$ ) on the total energy of the  $\text{Ag}_{1-c}\text{Zn}_c$  alloys in the bcc crystal structure. The slope of  $\Delta E(\varepsilon_o^2)$  at  $\varepsilon_o^2=0$  is proportional to the  $C_{44}$  elastic constant.

compare our theoretical results for the equilibrium volume, elastic constants, Every anisotropy, and Debye temperature to the available experimental data. The quoted experimental values for the elastic constants and Debye temperature from Ref. 29 have been extrapolated to  $T=0$  K by using the observed temperature dependences below 300 K.<sup>3,29</sup>

In Figs. 3 and 4 we present the theoretical lattice parameters  $a$  and bulk moduli  $B$  calculated for the  $\text{Ag}_{1-c}\text{Zn}_c$  alloys in the fcc and bcc phases. For comparison, former theoretical results<sup>30,31</sup> and experimental data for the lattice constants<sup>32</sup> and bulk moduli<sup>29</sup> are also shown. The errors in the theoretical ground-state parameters are typical for what has been obtained for simple metals and transition metals<sup>23,33</sup> in conjunction with the local density approximation for the

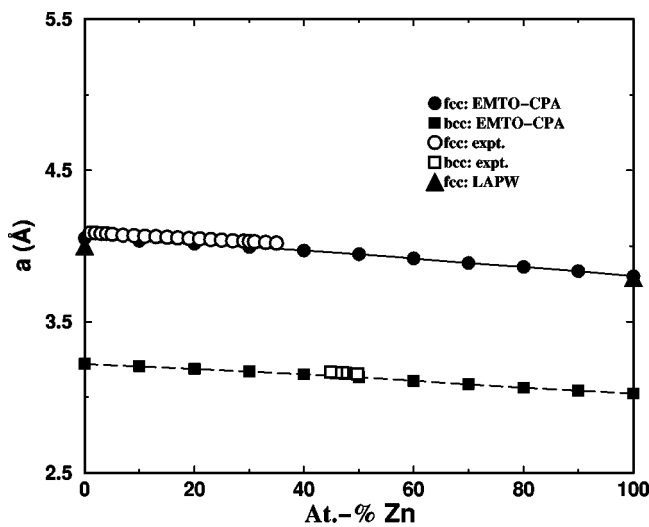


FIG. 3. Theoretical lattice constants of  $\text{Ag}_{1-c}\text{Zn}_c$  alloys in the fcc and bcc structures, calculated using the EMTO-CPA method (Ref. 4). The present values are compared with the experimental data (Ref. 32). For pure Ag and Zn the full potential results from Refs. 30 and 31 are also shown.

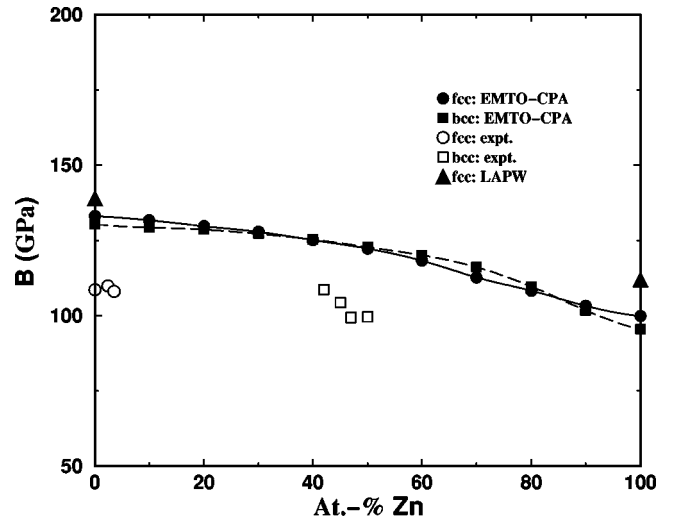


FIG. 4. Theoretical bulk moduli of  $\text{Ag}_{1-c}\text{Zn}_c$  alloys in the fcc and bcc structures, calculated using the EMTO-CPA method (Ref. 4). The present values are compared with the experimental data extrapolated to 0 K (Ref. 29). For pure Ag and Zn the full potential results from Refs. 30 and 31 are also shown.

exchange-correlation energy functional. The agreement between our results for fcc Ag and Zn and those calculated using the *linear augmented plane-wave* (LAPW) method<sup>30,31</sup> is reasonable. The relative differences in  $a$  and  $B$  are 1.3% and  $-4.3\%$  for Ag and 0.3% and  $-10.9\%$  for Zn, respectively. We note that for pure Ag the calculated volume per atom is 0.3% larger for the bcc lattice compared with that of the fcc lattice. For pure Zn the corresponding difference is 0.7%.

The theoretical and experimental elastic constants  $C'$  and  $C_{44}$  are shown in Fig. 5. The open symbols refer to experimental data from the Landolt-Börnstein tables<sup>3</sup> ( $\alpha$  phase) and Murakami and Kachi<sup>29</sup> ( $\beta$  phase). For both elastic constants the present results are in excellent agreement with the experimental values. For pure Ag the theoretical elastic parameters calculated using the full potential LAPW and *linear muffin-tin orbitals* (LMTO) methods<sup>2,30,34</sup> are also included. If we take, as the error connected with such calculations, the difference between the LAPW and LMTO results, i.e.,  $\sim 5$  GPa for  $C'$  and  $\sim 9$  GPa for  $C_{44}$ , the agreement between the present and former theoretical results is very good.

The variation of the bulk modulus with the Zn concentration is smooth in both crystal structures. However, a quite different behavior is observed in the case of  $C'$  and  $C_{44}$ . For instance,  $C'_{\text{bcc}}$  is drastically reduced above  $c \approx 0.78$ , where, in fact, this system reaches a dynamical instability. At the same time, at large Zn content the fcc Ag-Zn is strongly stabilized against tetragonal shear. On the other hand,  $C_{44}$  has almost constant values for  $c \leq 0.5$  and  $c \leq 0.7$  in the fcc and bcc structures, respectively. Above these concentration ranges  $C_{44}$  shows rapid variation in both structures, describing a trend from stable structures (Ag end) towards unstable (bcc) or barely stable (fcc) structures (Zn end). The instability of fcc Zn against orthorhombic deformations has also been reported in other theoretical investigations.<sup>31</sup>

When a comparison can be made between experiments

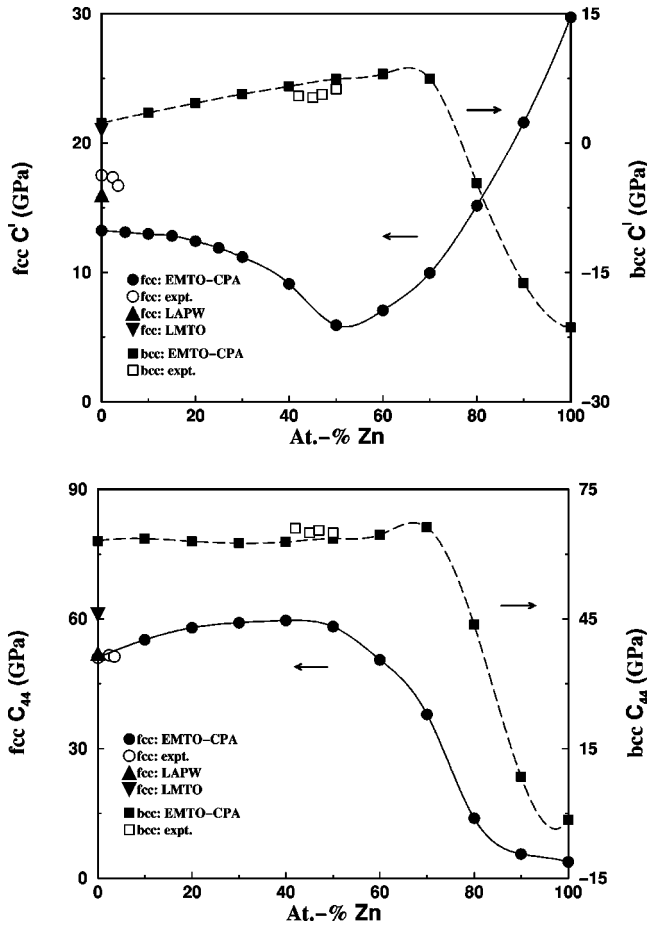


FIG. 5. Theoretical elastic constants ( $C'$  and  $C_{44}$ ) of  $\text{Ag}_{1-c}\text{Zn}_c$  alloys in the fcc and bcc structures, calculated using the EMTO-CPA method (Ref. 4). The present values are compared with the experimental data extrapolated to 0 K (Ref. 29). For pure Ag and Zn the full potential results from Ref. 2 (LMTO) and Ref. 34 (LAPW) are also shown.

and our results for the elastic constants, the agreement is very good. We therefore have confidence in our data also when they show an anomalous behavior. The abruptness of the variations in  $C'$  and  $C_{44}$  is more pronounced than has been reported in any experiments for nonmagnetic solids.<sup>3</sup> The often-used “law of mixing” for the shear moduli, i.e., a linear variation between the values at the end members in the alloy, definitely fails in the case of Ag-Zn alloys. Rapid, but smaller, variations of elastic constants as a function of composition or temperature have been noted for several transition-metal alloys<sup>3</sup> and attributed to topological Fermi-surface transitions.<sup>35</sup>

The enthalpy of formation of  $\text{Ag}_{1-c}\text{Zn}_c$  alloy for an arbitrary crystal structure is calculated as

$$\Delta H(c) = E(\text{Ag}_{1-c}\text{Zn}_c) - (1-c)E_{\text{fcc}}(\text{Ag}) - cE_{\text{hcp}}(\text{Zn}), \quad (9)$$

where all the energies are obtained for the calculated equilibrium volume and expressed per atom.  $E_{\text{fcc}}(\text{Ag})$  and  $E_{\text{hcp}}(\text{Zn})$  are the total energies of fcc Ag and hcp Zn, respectively. The solid solution of the Ag-Zn system is formed

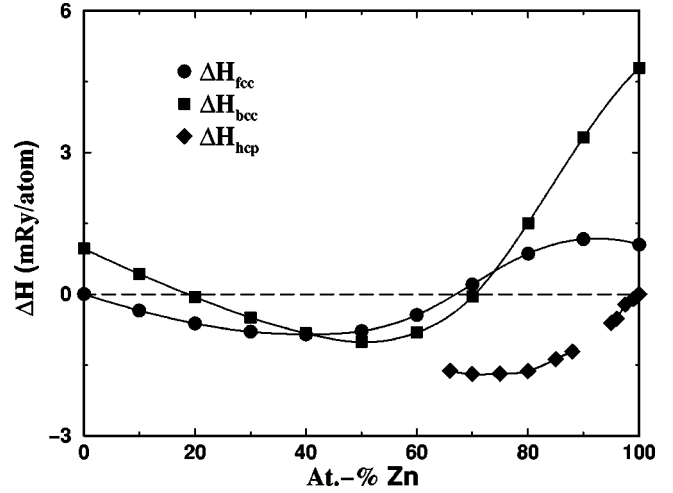


FIG. 6. The enthalpy of formation of  $\text{Ag}_{1-c}\text{Zn}_c$  alloys in the fcc, bcc, and hcp structures calculated using the EMTO-CPA method (Ref. 4).

when  $\Delta H(c) < 0$ . In Fig. 6 we present  $\Delta H_{\text{fcc}}(c)$  and  $\Delta H_{\text{bcc}}(c)$  as functions of the alloy composition. For reference, we also include the enthalpy of formation calculated for the experimental  $\epsilon$  and  $\eta$  phases [ $\Delta H_{\text{hcp}}(c)$ ]. These phases are observed for  $0.66 \leq c \leq 0.89$  and for  $c > 0.95$ , and have hcp structure with  $c/a \approx 1.56$ , and  $c/a \approx 1.8$ , respectively.<sup>36</sup> A comparison between the bcc, fcc, and hcp enthalpies shows the relative stability of the fcc phase below 0.4 and of the hcp phases above 0.6 Zn content. This is in qualitative agreement with the phase diagram from Fig. 1. However, we note that entropy effects must also be considered in a full account of the high temperature phase diagram. Analyzing Figs. 1 and 6 we point out that the bcc structure at concentrations  $c \sim 0.4$  will be further stabilized over the fcc structure at high temperatures by the entropy contribution to the configurational part of the Gibbs energy.

In studies<sup>1,2</sup> of elastic constants of transition metals, a correlation between  $C'$  and the energy difference between the bcc and fcc structures,  $\Delta E_{\text{bcc-fcc}} \equiv E_{\text{bcc}} - E_{\text{fcc}}$ , was proposed. In the case of Ag-Zn alloys  $\Delta E_{\text{bcc-fcc}}(c)$  first decreases from 0.9 mRy ( $c=0$ ) to  $-0.5$  mRy ( $c=0.6$ ) and then increases to 3.6 mRy ( $c=1$ ). This trend correlates reasonably well with both  $C'_{\text{fcc}}$  and  $-C'_{\text{bcc}}$ . However, a much better correlation exists between  $\Delta E_{\text{bcc-fcc}}(c)$  and the difference between the two tetragonal shear moduli. At small Zn concentrations  $C'_{\text{fcc}}$  decreases and  $C'_{\text{bcc}}$  increases with  $c$ , suggesting the stabilization of the bcc phase against the fcc phase. In the region between 45 and 65 at. % Zn the  $C'_{\text{bcc}}$  becomes slightly larger than the  $C'_{\text{fcc}}$ , showing a pronounced energy minimum for the bcc phase. Above 65 at. % Zn one has  $C'_{\text{fcc}} > C'_{\text{bcc}}$ , and a restabilization of the fcc structure, relative to the bcc structure, occurs.

In the upper panel of Fig. 7 the Every anisotropies are shown for the fcc and bcc structures. The open symbols refer to experimental data for the  $\alpha$  (Ref. 37) and  $\beta$  (Refs. 29 and 38) phases. For Ag-rich alloys the theoretical anisotropies, calculated from Eq. (2), are in good agreement with the experimental values. The somewhat worse agreement for the

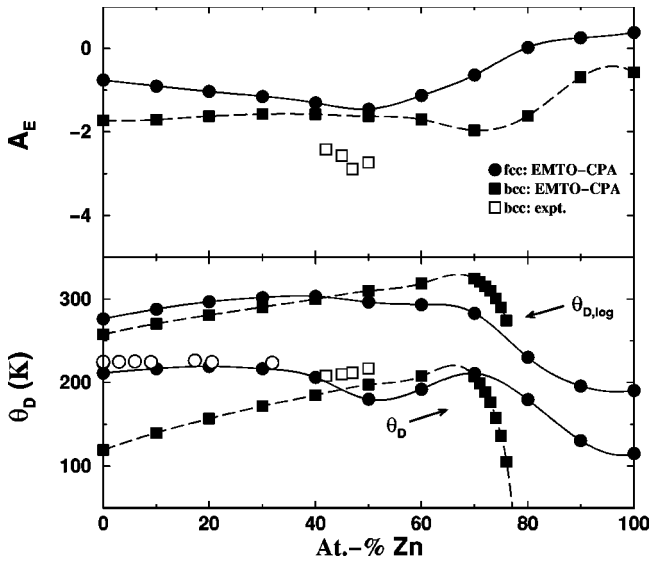


FIG. 7. Theoretical elastic anisotropies (upper panel) and Debye temperatures (lower panel) of  $\text{Ag}_{1-c}\text{Zn}_c$  alloys in the fcc and bcc structures calculated using the EMTO-CPA method (Ref. 4). The lower curves for the Debye temperature ( $\theta_D$ ) refer to the values obtained from the average of the sound velocities, Eq. (3), and the upper curves ( $\theta_{D,\log}$ ) to the values obtained from the logarithmic average of the sound velocities, Eq. (4). The low-temperature experimental data are taken from Refs. 37 (for the fcc structure) and 29 (for the bcc structure).

bcc structure may be due to the fact that the experimental values were measured for ordered phases. The extreme values of anisotropies are observed at  $\sim 50$  and  $\sim 70$  at. % Zn for the fcc and bcc structures, respectively. For the  $\eta$  phase we find almost isotropic values in both structures. We note that the bcc structure, for all concentrations, has a larger anisotropy when compared with the fcc structure.

The lower panel of Fig. 7 presents the Debye temperatures as calculated from Eqs. (3) and (4). Since these Debye temperatures are not defined for dynamically unstable lattices, they are shown only for  $c \leq 0.76$  in the case of the bcc structure. For reference, the available low-temperature experimental values are also included for the fcc (Ref. 37) and bcc (Ref. 29) structures. The agreement between experimen-

tal and theoretical Debye temperatures, including the concentration dependence, is very good. The quantity  $\theta_D$  goes to zero as one approaches  $c_{\text{crit}}$ , while  $\theta_{D,\log}$  has a finite limiting value. The difference is due to the fact that  $\theta_D$  is essentially obtained from the average of  $\omega^{-3}$ , while  $\theta_{D,\log}$  from the average of  $\ln \omega$ , where  $\omega$  denotes the vibrational frequencies. This behavior of  $\theta_D$  and  $\theta_{D,\log}$  is mathematically exact for harmonic vibrations. In a real system it will be somewhat modified because also the vibrational displacement diverges at  $c_{\text{crit}}$ , thus giving rise to anharmonic effects at concentrations near  $c_{\text{crit}}$ . However, it is striking in Fig. 7 how narrow the region of rapid variation in  $\theta_D$  and  $\theta_{D,\log}$  is.

The vibrational Gibbs energy  $G$ , at high temperatures, depends primarily on  $\ln \theta_{D,\log}$ .<sup>21</sup> Therefore  $G$  is still well behaved near  $c_{\text{crit}}$ . As a consequence, a phase diagram will not show any anomalies near  $c_{\text{crit}}$  that relate to the corresponding unstable phase.<sup>21</sup>

#### IV. CONCLUSIONS

Using the EMTO-CPA *ab initio* total energy method we have determined the elastic properties of the random Ag-Zn binary alloys. Good agreement is found with the available experimental data. We obtain rapid variations in the  $C'$  and  $C_{44}$  elastic constants of high Zn content alloys. The fcc structure shows strong elastic anisotropy at concentrations around 50 at. % Zn, and the bcc structure becomes approximately isotropic only near the Zn end. We predict that the bcc Ag-Zn alloys with high Zn concentrations are dynamically unstable and the corresponding fcc alloys are just barely stable.

#### ACKNOWLEDGMENTS

The Swedish Natural Science Research Council, the Swedish Foundation for Strategic Research, and the Royal Swedish Academy of Sciences are acknowledged for financial support. Part of this work was supported by research project No. OTKA T035043 of the Hungarian Scientific Research Fund and by the Hungarian Academy of Science. The calculations were performed at the Swedish National Supercomputer Center, Linköping, and the Hungarian National Supercomputer Center, Budapest.

<sup>1</sup>J. M. Wills, O. Eriksson, P. Söderlind, and A. M. Boring, Phys. Rev. Lett. **68**, 2802 (1992).

<sup>2</sup>P. Söderlind, O. Eriksson, J. M. Wills, and A. M. Boring, Phys. Rev. B **48**, 5844 (1993).

<sup>3</sup>A. G. Every and A. K. McCurdy, in *Low Frequency Properties of Dielectric Crystals: Elastic Constants*, edited by D. F. Nelson, Landolt-Börnstein New Series, Group III, Vol. 29, Pt. a (Springer-Verlag, Berlin, 1992), p. 1.

<sup>4</sup>L. Vitos, I. A. Abrikosov, and B. Johansson, Phys. Rev. Lett. **87**, 156401 (2001).

<sup>5</sup>W. Hume-Rothery, *The Metallic State* (Oxford University Press, New York, 1931).

<sup>6</sup>P. Hohenberg and W. Kohn, Phys. Rev. **136**, B864 (1964).

<sup>7</sup>W. Kohn and L. J. Sham, Phys. Rev. **140**, A1133 (1965).

<sup>8</sup>O. K. Andersen, O. Jepsen, and G. Krier, in *Lectures on Methods of Electronic Structure Calculations*, edited by V. Kumar, O. K. Andersen, and A. Mookerjee (World Scientific, Singapore, 1994), p. 63.

<sup>9</sup>O. K. Andersen, C. Arcangeli, R. W. Tank, T. Saha-Dasgupta, G. Krier, O. Jepsen, and I. Dasgupta, in *Tight-Binding Approach to Computational Materials Science*, edited by P. E. A. Turchi, A. Gonis, and L. Colombo, MRS Symposia Proceedings No. 491 (Materials Research Society, Pittsburgh, 1998), p. 3.

<sup>10</sup>O. K. Andersen, T. Saha-Dasgupta, R. W. Tank, C. Arcangeli, O. Jepsen, and G. Krier, in *Electronic Structure and Physical Properties of Solids: The uses of the LMTO method*, edited by H.

- Dreyssé, Lectures Notes in Physics (Springer-Verlag, Berlin, 2000), p. 3.
- <sup>11</sup>O. K. Andersen and T. Saha-Dasgupta, Phys. Rev. B **62**, R16 219 (2000).
- <sup>12</sup>L. Vitos, H. L. Skriver, B. Johansson, and J. Kollár, Comput. Mater. Sci. **18**, 24 (2000).
- <sup>13</sup>L. Vitos, Phys. Rev. B **64**, 014107 (2001).
- <sup>14</sup>P. Soven, Phys. Rev. **156**, 809 (1967).
- <sup>15</sup>B. L. Györfy, Phys. Rev. B **5**, 2382 (1972).
- <sup>16</sup>L. Vitos, I. A. Abrikosov, and B. Johansson (unpublished).
- <sup>17</sup>J. Kollár, L. Vitos, and H. L. Skriver, in *Electronic Structure and Physical Properties of Solids: The uses of the LMTO method*, edited by H. Dreyssé, Lectures Notes in Physics (Springer-Verlag, Berlin, 2000), p. 85.
- <sup>18</sup>G. A. Alers and J. R. Neighbours, J. Appl. Phys. **28**, 1514 (1957).
- <sup>19</sup>A. G. Every, Phys. Rev. B **22**, 1746 (1980).
- <sup>20</sup>G. Grimvall, *Thermophysical Properties of Materials, enlarged and revised ed.* (North-Holland, Amsterdam, 1999).
- <sup>21</sup>G. Grimvall, in *CALPHAD and Alloy Thermodynamics*, edited by P. E. A. Turchi, A. Gonis, and R. D. Shull (The Minerals, Metals and Materials Society, Warrendale, 2002), p. 81.
- <sup>22</sup>P. A. Korzhavyi, A. V. Ruban, I. A. Abrikosov, and H. L. Skriver, Phys. Rev. B **51**, 5773 (1995).
- <sup>23</sup>L. Vitos, B. Johansson, J. Kollár, and H. L. Skriver, Phys. Rev. B **62**, 10 046 (2000).
- <sup>24</sup>L. Vitos, B. Johansson, and J. Kollár, Phys. Rev. B **62**, R11 957 (2000).
- <sup>25</sup>B. Magyari-Köpe, L. Vitos, and J. Kollár, Phys. Rev. B **63**, 104111 (2001).
- <sup>26</sup>B. Magyari-Köpe, L. Vitos, B. Johansson, and J. Kollár, Acta Crystallogr., Sect. B: Struct. Sci. **57**, 491 (2001).
- <sup>27</sup>J. P. Perdew and Y. Wang, Phys. Rev. B **45**, 13 244 (1992).
- <sup>28</sup>V. L. Moruzzi, J. F. Janak, and K. Schwarz, Phys. Rev. B **37**, 790 (1988).
- <sup>29</sup>Y. Murakami and S. Kachi, Jpn. J. Appl. Phys., Part 1 **13**, 1728 (1974).
- <sup>30</sup>A. Khein, D. J. Singh, and C. J. Umrigar, Phys. Rev. B **51**, 4105 (1995).
- <sup>31</sup>S. Müller, L. W. Wang, A. Zunger, and C. Wolverton, Phys. Rev. B **60**, 16 448 (1999).
- <sup>32</sup>W. B. Pearson, *A Handbook of Lattice Spacings and Structures of Metals and Alloys* (Pergamon, Oxford, 1964), Vol. 4.
- <sup>33</sup>S. Kurth, P. J. Perdew, and P. Blaha, Int. J. Quantum Chem. **75**, 889 (1999).
- <sup>34</sup>M. J. Mehl and D. A. Papaconstantopoulos, Phys. Rev. B **54**, 4519 (1996).
- <sup>35</sup>E. Bruno, B. Ginatempo, E. S. Giuliano, A. V. Ruban, and Yu. Kh. Vekilov, Phys. Rep. **249**, 353 (1994).
- <sup>36</sup>T. B. Massalski, J. Phys. Radium **23**, 647 (1962).
- <sup>37</sup>B. A. Green, Jr., Phys. Rev. **144**, 528 (1966).
- <sup>38</sup>J. P. Abriata, O. J. Bressan, C. A. Luengo, and D. Thoulouze, Phys. Rev. B **2**, 1464 (1970).
- <sup>39</sup>T. Massalski, *Binary Alloys Phase Diagrams* (ASM, Metals Park, OH, 1990), p. 117.